JPE 18-3-28

https://doi.org/10.6113/JPE.2018.18.3.944
ISSN(Print): 1598-2092 / ISSN(Online): 2093-4718

Modeling and Analysis of SEIG-STATCOM Systems Based on the Magnitude-Phase Dynamic Method

Haifeng Wang*, Xinzhen Wu†, Rui You*, and Jia Li*

†,*Department of Electrical Engineering, Qingdao University, Qingdao, China

Abstract

This paper proposes an analysis method based on the magnitude-phase dynamic theory for isolated power systems with static synchronous compensators (STATCOMs). The stability margin of an isolated power system is greatly reduced when a load is connected, due to the disadvantageous features of the self-excited induction generators (SEIGs). To analyze the control process for system stability and to grasp the dynamic characteristics in different timescales, the relationships between the active/reactive components and the phase/magnitude of the STATCOM output voltage are derived in the natural reference frame based on the magnitude/phase dynamic theory. Then STATCOM equivalent mechanical models in both the voltage time scale and the current time scale are built. The proportional coefficients and the integral coefficients of the control process are converted into damping coefficients, inertia coefficients and stiffness coefficients so that analyzing its controls, dynamic response characteristics as well as impacts on the system operations are easier. The effectiveness of the proposed analysis method is verified by simulation and experimental results.

Key words: Magnitude/phase dynamics, Self-excited induction generator, Static synchronous compensator (STATCOM), Time scale, Voltage regulation

I. INTRODUCTION

Distributed generation has been identified as a new trend to accommodate various renewable energies, due to its power supply reliability in remote locations, environmental friendliness, reduced construction costs and ease of reactive power compensation [1]. Isolated power systems, such as micro-grid systems and the on-board isolated power supply systems, are among the most important applications of distributed generations [2], [3]. In these applications, Self-Excited Induction Generators (SEIGs) have always been appealing research topics, due to their advantageous features in terms of operation and maintenance simplicity and self-protection against faults, etc. [4]-[7]. However, the major problem with isolated power systems is poor voltage regulation with prime mover speed variations and a load connected to a SEIG. When a SEIG is driven by bio-gas/diesel engines, it is operated at a constant speed. Therefore, the generation frequency is less affected by load perturbations, but the terminal voltage is barely kept at its rated value when the reactive power requirement increases [8], [9].

In addition, the magnetizing reactive power is supplied by connecting excitation capacitors with stator windings. To solve the above problems, the extra reactive power of a system needs to be compensated within the limits of load changes. A number of schemes have been investigated in the last two decades [10]-[19]. The main methods can be summarized as follows.

Method I: self-regulating using passive components such as series capacitors. The load-carrying capacity of induction generators can be improved by shunt compensation capacitors. However, such schemes can result in Sub-Synchronous Resonance (SSR) during the starting connection and they are highly affected by the nature of the load [10].

Method II: voltage can be regulated by a load controller or

Manuscript received Jun. 26, 2017; accepted Jan. 9, 2018
Recommended for publication by Associate Editor Seon-Hwan Hwang.
†Corresponding Author: wuxinzhen81@163.com
Tel: +86-532-58950695, Qingdao University
*College of Automation and Electrical Engineering, Qingdao University, China

a Static Var Compensator (SVC) consisting of active components, reactors and capacitors [11]. Generally, a SVC is composed of Thyristor Controlled Reactors (TCRs), Thyristor Switched Capacitors (TSCs), or both. Due to the limitation of shunt reactors or the shunt capacitance impedance characteristic, the main disadvantage of this method is the narrow compensation operation range and the injection of low-frequency harmonics [12].

Method III: voltage source inverter (VSI) based design of static synchronous compensators (STATCOMs) has been implemented in [13]. These STATCOMs can be used to overcome compensating problems such as imbalances of the power factor and current, as well as current harmonics to achieve a balanced sinusoidal current at the line. The performance of STATCOMs is improved with the development of power electronic devices and control chips, such as IGBTs and DSPs [14]. Unlike SVCs, STATCOMs do not inject harmonics into the system. Moreover, they exhibit a superior dynamic response. Mithulananthan et al. have described the benefits of STATCOMs over SVC systems [15].

In isolated power systems with shunt-connected SEIGs and STATCOMs, the principle of operation for reactive power compensation is based on the current control of the connection inductor between the STATCOM and the SEIG to a desired order for the system, as shown in Fig. 1. The compensation current is injected at the point of the common coupling. Under different load conditions, Singh et al. proposed a simple mathematic model for the transient analysis of the SEIG–STATCOM system under balanced/ unbalanced three-phase and single-phase nonlinear loads [16], [17]. In [18], a fuzzy proportional-integral (PI) based voltage control scheme was proposed. It yielded a superior response under balanced and unbalanced loading cases. When compared with the conventional PI method, the latter has better capability in terms of voltage regulation. Moreover, the current synchronous detection (CSD) method and a modified method were proposed to enhance the harmonic suppression capability of nonlinear loads, and their feasibilities were verified by simulation and experimental results [19]. However, the given methods only concentrated on new control schemes and optimizations, while the analysis of different timescale physical relationships of equipment was ignored.

In [20], a magnitude/phase dynamic method based on multi-time scales was proposed, and the dynamic processes of different timescales were analyzed under a novel concept using mechanic motion equations. Multi-time scale control interaction is the essential difference of dynamic stability problems between power electronics dominated power systems and traditional electromagnetic devices dominated power systems. The magnitude/phase dynamic method is a generalization concept, which describes the physical characteristics of power conversion devices and networks. From a mechanical point of view, the voltage or current response processes are equivalent to motion equations. In this paper, the magnitude/phase dynamic method is used to model and analyze SEIG-STATCOM systems. This paper makes an analytical analogy between the motion equations of the magnitude/phase and the mechanical spring/rotor. In addition, it obtains a corresponding relationship between the control parameters and the moment of inertia/damping. Mechanical models in different timescale control processes have been built. They can be used to make system commissioning more convenient. Experiments and applications can refer to the rotor/spring dynamic response when changing the control parameters and dynamic performance of a STATCOM device.

It is necessary to point out that the SEIG voltage regulation problem has been solved. In this paper, this example is used to illustrate the application of the magnitude/phase dynamic method in an actual SEIG isolated system with a STATCOM. This method shows the physical mechanism of the device operation. It is convenient to grasp the dynamic characteristics of the STATCOM in different timescales and to estimate the influence of these characteristics on system stability in order to regulate the dynamic characteristics [21]. In addition, the state model can be simplified according to the time constant of the method. For example, the steady-state can be considered when the time constant is large.

This paper is organized as follows. First, a SEIG-STATCOM system is introduced, and the modeling of the SEIG is provided. Then, timescale classification of the system is illustrated, and the magnitude/phase motion equations of different timescales are proposed. Finally, simulation and experimental results that demonstrate the accuracy of the proposed model and analysis are presented.

II. System Structure and Modeling

A schematic diagram of a SEIG isolated power system with a STATCOM is illustrated in Fig. 1. At the stator side of the generator, there is an excitation capacitor bank in parallel with the STATCOM and the load. The shunt excitation capacitors have fixed values to build a rated terminal voltage at no load. Therefore, an adequate steady state is carried out with the three phase circuits of the SEIG [22]. A reactive power supply is delivered from the excitation capacitors and STATCOM. In order to regulate the compensated system voltage and power, an injection current control is achieved by means of the STATCOM connected to the generator terminals. In this system, a DC motor is used to drive the rotor as the prime mover at a constant speed before and after load switching. Therefore, the generation frequency is less affected by load changes. The STATCOM is composed of a three-phase IGBT-based inverter and a DC bus capacitor. The

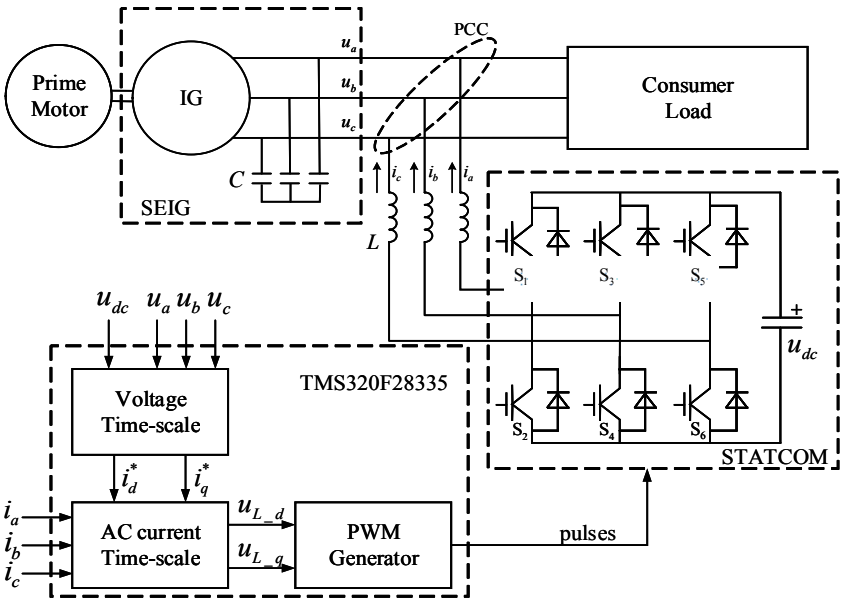

Fig. 1. Schematic diagram of a SEIG-STATCOM isolated power system.

output of the STATCOM is paralleled with the AC filtering inductor to the SEIG terminals. The pulse width or duty cycle of the chopper is decided by the difference of the reactive power requirement.

A. Modeling of the SEIG

The mutual inductance matrix is a non-linear time-varying parameter due to the interaction between the stator and the rotor via the magnetic field coupling. Therefore, the SEIG is modeled using the *d-q* axis rotating reference frame, where the mutual inductance matrix is a time-invariance parameter with a decoupling calculation.

The voltage and current equations of an induction generator in the rotating *d-q* reference frame are given as:

$$pi = Ai + Bu \tag{1}$$

$$A = K\begin{bmatrix} -R_S L_R & \omega L_M^2 & R_R L_M & \omega L_M L_R \\ -\omega L_M^2 & -R_S L_R & -\omega L_M L_R & R_R L_M \\ R_S L_M & -\omega L_M L_S & -R_R L_R & -\omega L_S L_R \\ \omega L_M L_S & R_S L_M & \omega L_S L_R & -R_R L_R \end{bmatrix} \tag{2}$$

$$B = K\begin{bmatrix} L_R & 0 \\ 0 & L_R \\ -L_M & 0 \\ 0 & -L_M \end{bmatrix} \tag{3}$$

where 'p' represents the derivative with respect to time, R_S is the stator resistance, R_R is the rotor resistance, L_S is the stator inductance, L_R is the rotor inductance, L_M is the magnetizing inductance, ω is the rotor angular velocity. In addition:

$$i = [i_{ds}\ \ i_{qs}\ \ i_{dr}\ \ i_{qr}]^T \tag{4}$$

$$u = [u_{ds}\ \ u_{qs}]^T \tag{5}$$

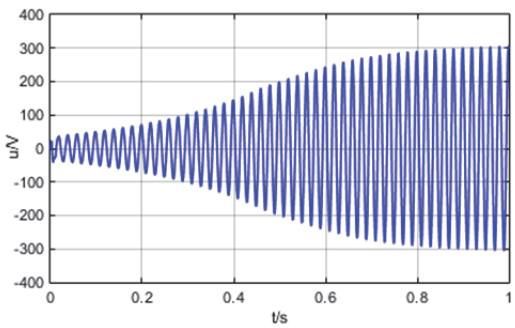

Fig. 2. Voltage waveform of a SEIG with a 30μF capacitor per phase.

$$K = \frac{1}{L_S L_R - L_M^2} \tag{6}$$

where i_{ds} and i_{qs} are the stator currents on the *d*-axis and *q*-axis, i_{dr} and i_{qr} are the rotor currents on the *d*-axis and *q*-axis, u_{ds} and u_{qs} are the stator voltages on the *d*-axis and *q*-axis, respectively. The magnetizing inductance varies with the variation of the magnetic saturation circuit. The SEIG operates in the saturation region and its magnetizing current is determined by the stator and rotor currents i_{ds}, i_{dr}, i_{qs} and i_{qr} using the following expression [23]:

$$i_m = \sqrt{(i_{ds} + i_{dr})^2 + (i_{qs} + i_{qr})^2} \tag{7}$$

Fig. 2 shows a generator voltage waveform built at 30μF excitation capacitors. The capacitors are connected with the SEIG terminal in a star connection. For this induction generator, 30μF is the minimum of the excitation capacitor, and the rated terminal voltage is built-up at no load. The frequency is keep at 50Hz with the SEIG operating at a normal degree of saturation and a constant prime motor speed.

B. Structure of the STATCOM

Fig. 1 shows that a STATCOM is a current controlled voltage source pulse width modulated inverter. The condition of the DC voltage for the STATCOM normal operation is given as:

$$U_{dc} > \sqrt{2}\sqrt{3}U_S = 2.45U_S = 2.45 \times 220 = 539V \quad (8)$$

where U_S is the peak voltage of the isolated power system, which is also the SEIG terminal voltage u_t:

$$u_t = \sqrt{\frac{2}{3}(u_a^2 + u_b^2 + u_c^2)} \quad (9)$$

Fig. 3 shows a phase equivalent circuit of the STATCOM. u_I is the output voltage of the device whose magnitude and phase are only controlled under the fundamental frequency. u_L is the voltage of the inductor L, which is the vector difference between u_I and u_S. The active power loss of the device is considered as the resistance R. i is the current of one phase.

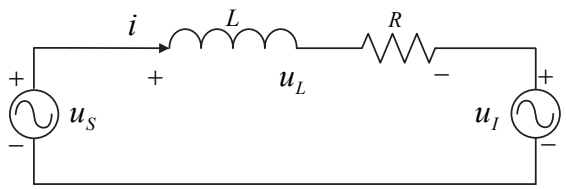

Fig. 3. Phase equivalent circuit of a STATCOM.

The voltage of the inductor is computed as:

$$u_L = L\frac{\mathrm{d}i}{\mathrm{d}t} + Ri \quad (10)$$

$$u_L = u_S - u_I \quad (11)$$

According to the principle of the STATCOM, the magnitude and phase of u_L determine the property and magnitude of the compensation power.

III. Magnitude and Phase Motion Equations of the STATCOM

A. Multi-Time Scale

As presented in Section I, the SEIG-STATCOM system includes different timescales. The time constants are different according to the control loops. For example, the time constants of the rotor speed control, the dc-voltage control and the current control are about 1s, 100ms and 10ms, respectively [24]. The timescales of the different control loops in the SEIG-STATCOM system can be briefly classified as shown in Fig. 4.

The control scheme regulating the power compensation of the SEIG system is based on the output voltage of the STATCOM. Fig. 4 shows the multi-time scale control of a SEIG-STATCOM system. In this system, the rotor speed control is of the large time scale (more than 1s) due to the rotor inertia and slow response. The DC voltage and the terminal voltage are of the middle level time scale (about 100ms to 1s). The alternating-current is of the small level time scale (less than 100ms), which is also the electromagnetic time scale in conventional power systems. In this paper, the rotor speed is kept constant. There are motion equations in the different timescales. The equations are equivalent to the mechanical spring and the mechanical rotor, which describe the control processes of the reactive and active components. Furthermore, the reactive and active components determine the phase and magnitude of $\dot{U}_{\mathrm{I}}$.

B. Voltage Time Scale

The magnitude and phase equations of the voltage time scale are illustrated in Fig. 5. The terminal voltage magnitude u_t is calculated by (9). In order to find the reactive component of the reference source current, a PI controller is used. The reference u_t^* and the actual measured terminal voltage are input variables for the PI controller, where the error is computed with the input variables, and the output reactive component reference i_q^* is obtained. The dynamic response of the control process is equal to a mechanical spring with a stiffness coefficient and a damped coefficient. The equivalent spring is described by:

$$i_q^* = H(K_{p\_t} + \frac{K_{i\_t}}{Ts})(\frac{u_t^*}{H} - u_t) \quad (12)$$

where K_{p_t} and K_{i_t} are the proportional gain and integral gain of the PI controller, respectively. In addition, H is the terminal voltage sampling coefficient, T is the time constant, HK_{p_t} is the equivalent damped coefficient, and HK_{i_t}/T is the equivalent stiffness coefficient.

In the equivalent spring model, the elastic force is the sum of the damped coefficient × velocity and the stiffness coefficient × displacement. The deviation of u_t^*/H_{dc} and u_t is considered as the displacement. For a mechanical spring, stiffness is the coefficient of the displacement, damping is the coefficient of the velocity, and displacement is the integral of the velocity. Therefore, the stiffness is related to the integral constant.

In order to get the active component of the reference source current, the voltage across the DC capacitor u_{dc} is sensed and sent to the PI controller. The error between u_{dc} and the reference variable u_{dc}^* is processed through a digital PI controller and the reactive component reference i_d^* is obtained. The one of the control process is similar to the one of a mechanical rotor with a rotary inertia and a damped coefficient. The equivalent rotor is described by:

$$i_d^* = H_{dc}(K_{p\_dc} + \frac{K_{i\_dc}}{Ts})(\frac{u_{dc}^*}{H_{dc}} - u_{dc}) \quad (13)$$

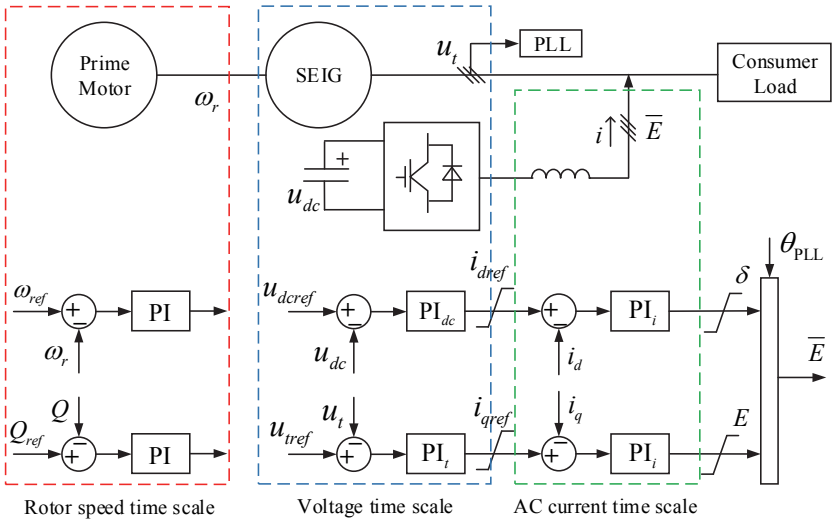

Fig. 4. Multi-time scale control of a SEIG-STATCOM system.

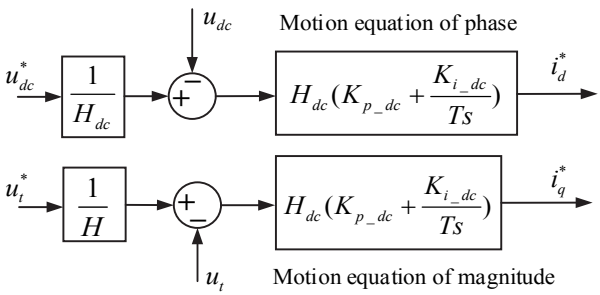

Fig. 5. Magnitude/phase equation of the voltage time scale.

where K_{p_dc} and K_{i_dc} are the proportional gain and integral gain of the PI controller, respectively. In addition, H_{dc} is the DC voltage sampling coefficient, $H_{dc}K_{i\_dc}/T$ is the equivalent damped coefficient, and $H_{dc}K_{p\_dc}$ is the equivalent rotary inertia.

In the equivalent rotor model, the torque is the sum of the rotary inertia × acceleration and the damped coefficient × velocity. The deviation of u_{dc}^{*}/H_{dc} and u_{dc} is considered as the acceleration of the angular velocity. For a mechanical rotor, damping is the coefficient of the velocity, rotary inertia is the coefficient of the acceleration, and velocity is the integral of the acceleration. Therefore, the damping is related to the integral constant.

In the active component, the phase-angle difference between $\dot{U}_{\mathrm{I}}$ and $\dot{U}_{\mathrm{S}}$ varies with the active power loss, and the three-phase IGBT-based inverter is unable to switch instantaneously. This characteristic is described by the phase motion equation and the mechanical rotor. In the reactive component, the equivalent spring describes the dynamic process of the voltage support after the load connection. The restoring force is described by the magnitude motion equation.

C. Alternating-Current Time Scale

The actual current is decoupled by Clark and Park transformations. The active and reactive components of the actual current is obtained in the *d-q* axis synchronous rotating reference frame. The output of the voltage time scale is the input reference variable in the AC current time scale where the active and reactive components of the STATCOM output voltage are computed through the PI controller. The control process is equivalent to motion equations of the AC time scale and is illustrated in Fig. 6.

The decoupled currents of the inductor are given as:

$$\begin{cases} L\dfrac{\mathrm{d}i_q}{\mathrm{d}t} = -(K_{p\_iq} + \dfrac{K_{i\_iq}}{Ts})(i_q^{*} - H_i i_q) - Ri_q \\ L\dfrac{\mathrm{d}i_d}{\mathrm{d}t} = -(K_{p\_id} + \dfrac{K_{i\_id}}{Ts})(i_d^{*} - H_i i_d) - Ri_d \end{cases} \tag{14}$$

where K_{p_iq} and K_{i_iq} are the proportional gain and integral gain of the reactive component PI controller, respectively. In addition, K_{p_id} and K_{i_id} are the proportional gain and integral gain of the active component PI controller, respectively. H_i is the AC sampling coefficient. In the AC time scale, the magnitude motion equation, which is equivalent to a spring, is described by:

$$u_{L\_q} = -(K_{p\_iq} + \frac{K_{\mathrm{i\_iq}}}{Ts})(i_q^{*} - H_i i_q) \tag{15}$$

The magnitude motion equation, which is the equivalent rotor, is described by:

$$u_{L\_d} = -(K_{p\_id} + \frac{K_{i\_id}}{Ts})(i_d^{*} - H_i i_d) \tag{16}$$

where $H_iK_{p\_iq}$ is the equivalent damped coefficient of the equivalent spring, $H_iK_{i\_iq}/T$ is the equivalent stiffness coefficient, $H_iK_{i\_id}/T$ is the equivalent damped coefficient of the equivalent rotor, and $H_iK_{p\_id}$ is the equivalent rotary

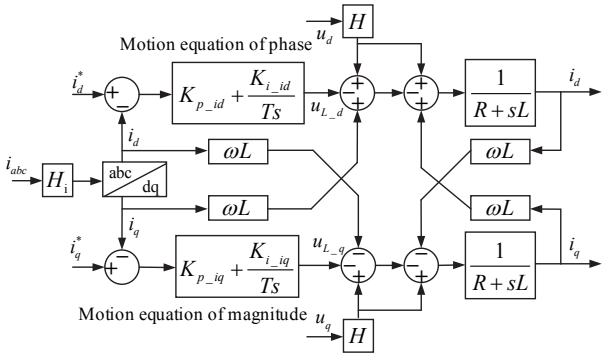

Fig. 6. Magnitude/phase equation of the AC time scale.

inertia. The analysis process of the coefficients is consistent with the preceding part of the text.

IV. Simulation and Experimental Results

A. Simulation Model

An isolate power system model composing of one induction generator with a fixed capacitor, one STATCOM and loads is built in Matlab/Simulink to verify the effectiveness of the proposed analysis method. In order to concentrate on the validation of the proposed analysis method, the balanced three-phase resistors are used as a load. The motor speed is set to constant, meaning that the system frequency remains approximately constant before and after the load connection. The structure of the simulation model is the same as that shown in Fig. 1.

For SEIG-STATCOM systems, one purpose of the control is to regulate the terminal voltage of the generator after load connection, and the terminal voltage is mainly controlled by the voltage time scale. Reactive power compensation for the voltage control is reflected in the supporting role of the q-axis reactive component. The supporting effect of the voltage can be equivalent to a spring from a mechanical perspective. According to (12), the damping coefficient of the spring is HK_{p_t}, and the stiffness coefficient is HK_{i_t}/T. Simulation results with the two parameters changed are shown in Fig. 7. With the constants H and T, the values of the parameters in Fig. 7 (a) are $K_{p\_t1}>K_{p\_t2}>K_{p\_t3}$, and the values of parameters in Fig. 7 (b) are $K_{i\_t1}>K_{i\_t2}>K_{i\_t3}$. The terminal voltage of the SEIG reflects the physical movement of the spring. In addition, the spring oscillation amplitude decreases when the damping coefficient increases. The spring rebound speed is larger when the stiffness coefficient increases. These results can show the physical mechanism of the device.

B. Experimental Platform

An isolated power system experimental platform was built. The STATCOM experimental prototype is illustrated in Fig. 8. The main parameters of the generator and STATCOM are shown in Table I. A 380V, 5A, 1450rpm induction machine is used as the prime mover as illustrated in Fig. 9. The

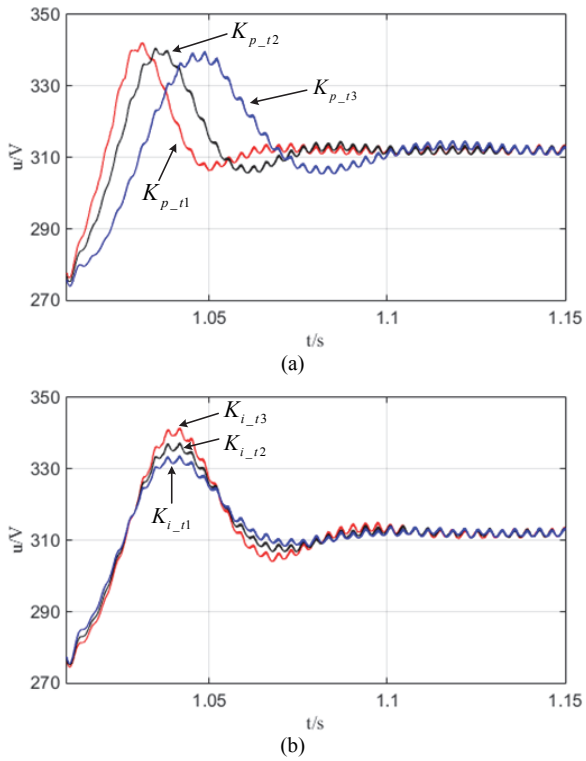

Fig. 7. Terminal voltage control in the voltage time scale. (a) Changes of the stiffness coefficient. (b) Changes of the damping coefficient.

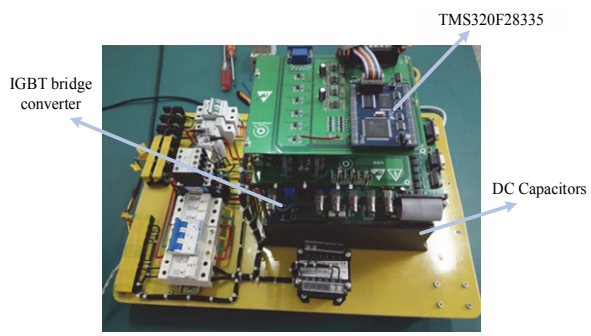

Fig. 8. STATCOM experimental prototype.

TABLE I
Main Parameters of Generator and Statcom

Parameters	Value	Parameters	Value
Power Rating/kW	2.2	Stator Leakage Inductance /H	0.0109
Rated Voltage/V	380	Rotor Resistance /Ω	3.200
Rated Speed/r/min	1500	Rotor Leakage Inductance /H	0.0109
Pole Pairs	2	Inductance L /mH	2
Rated Current/A	5	Rotor R/Ω	0.2
Stator Resistance /Ω	2.800	DC capacitor/μF	1000

excitation capacitors are in a star connection. Tests are carried out with a three-phase balanced resistive load.

The software is developed in Code Composer Studio (CCS), and it can be programmed and debugged online. In addition, it has a communication program between the computer, simulator

Fig. 9. SEIG experimental prototype.

TABLE II
CONTORL PARAMETERS OF DIFFERENT TIMESCALES

DC voltage scale parameter		Value	AC current scale parameter		Value
DC voltage	K_{p_dc}	0.3	Active Current	K_{p_id}	100
	K_{i_dc}	5		K_{i_id}	0
	H_{dc}	10		H_i	1
Terminal Voltage	K_{p_t}	0.2	Reactive Current	K_{p_iq}	100
	K_{i_t}	8		K_{i_iq}	0
	H	1		H_i	1

and power measurement modules.

The pulse output from the TMS320F28335 DSP is processed through a digitally isolated and intelligent power module driver. The pulses are given to the VSI in the STATCOM. The switches of the IGBT control the DC voltage of the capacitor and the current of the coupled inductor. The per phase EPWM driver of the DSP is taken from the dead band control for the positive and negative group conductions of the IGBT. The switching frequency is 10kHz. The controller coefficients are given in Table II.

C. Experimental Results

Fig. 10 illustrates transient waveforms of a balanced resistive load connection with the proposed model. The original waveform recorded by an oscillograph is shown in Fig. 10. The blue curve in Fig. 10(a) is the line voltage u_{ab}, and the yellow curve is the A-phase current i_{sa} of the generator. Because the generator is in a star connection, u_{ab} is 30 degrees ahead of i_{sa}. Fig. 10(b) is the dynamic response of the load switching. The load was connected and then removed after 1.5 seconds. The yellow curve is the compensation current i_a of the STATCOM.

During STATCOM operation, the compensation mode is constantly switching between capacitive and inductive. Fig. 11(a) shows an experimental waveform of the compensating capacitive reactive current. At this moment, the terminal voltage exceeded the reference value, and the STATCOM absorbed the reactive power. Fig. 11(b) is an experimental waveform of the compensating inductive reactive current. At this moment, the terminal voltage was less than the reference value, and the STATCOM emitted reactive power.

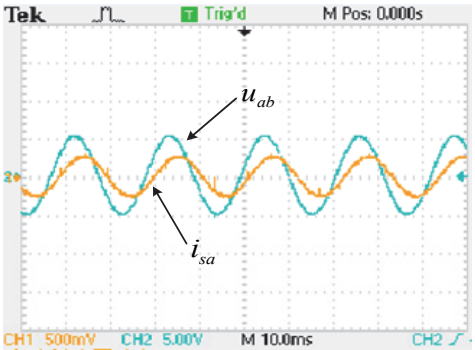

(a)

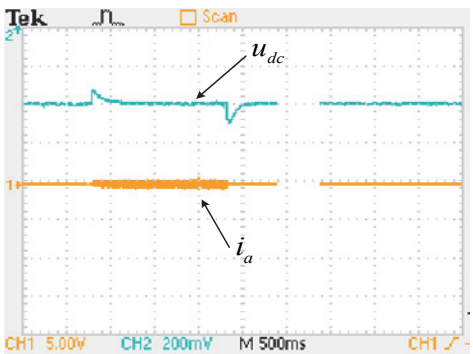

(b)

Fig. 10. Experimental waveforms. (a) Generator terminal voltage and current with a STATCOM. (b) STATCOM DC voltage and output current compensation during load connection and removal.

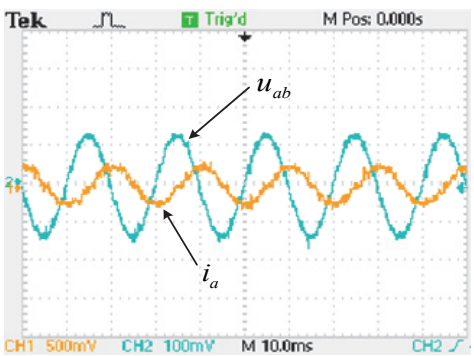

(a)

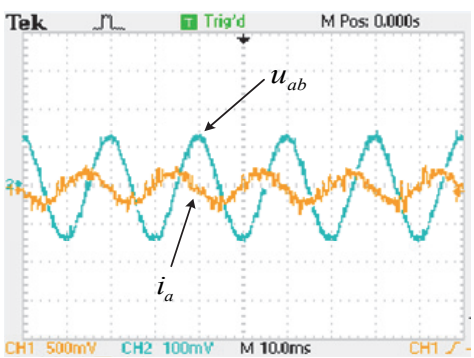

(b)

Fig. 11. Experimental waveforms under different operating conditions. (a) Capacitive current compensation. (b) Inductive current compensation.

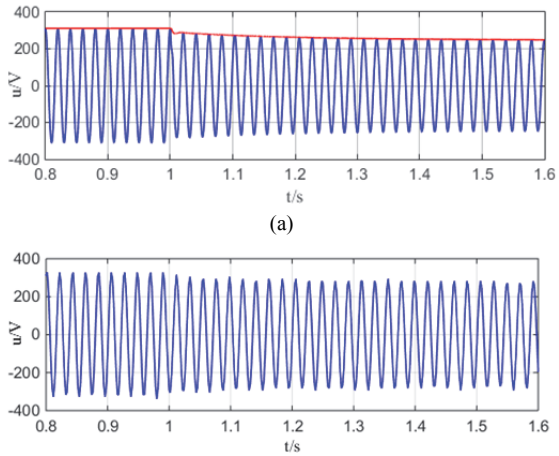

Fig. 12. Terminal voltage waveform without a STATCOM. (a) Waveform. (b) Waveform.

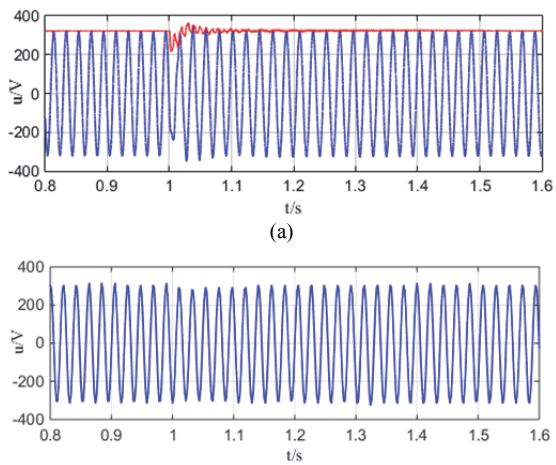

Fig. 13. Terminal voltage waveform with a STATCOM. (a) Simulation waveform. (b) Experimental waveform.

In order to display the experimental results better, the waveform data was recorded and drawn in MATLAB. Taking the A-phase voltage as an example, Fig. 12 illustrates the dynamic response process of the terminal voltage without the STATCOM. Then the results of the experiment and the simulation are compared. Generator voltage has been built-up, and system operated stably at 1s when a load was connected to the system. The terminal voltage dropped from 311V to 247V, and it fell more than 20% when the STATCOM device was not connected to the system. The red solid line is the terminal voltage magnitude.

Fig. 13 shows a system terminal voltage waveform with the STATCOM, and the results of the experiment and the simulation are compared. The STATCOM behaved as a source of reactive power when the load was connected. Meanwhile, a generator is utilized to charge the DC bus capacitor to a reference voltage of 700V and to supply the active power loss.

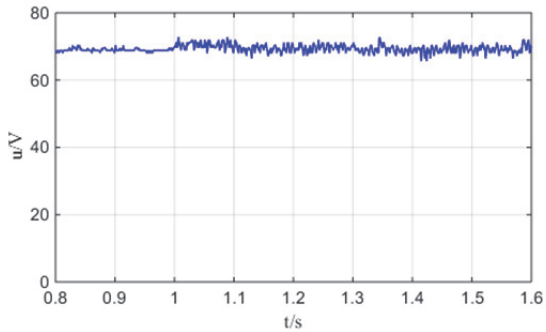

Fig. 14. Experimental waveform of the DC voltage after load connection.

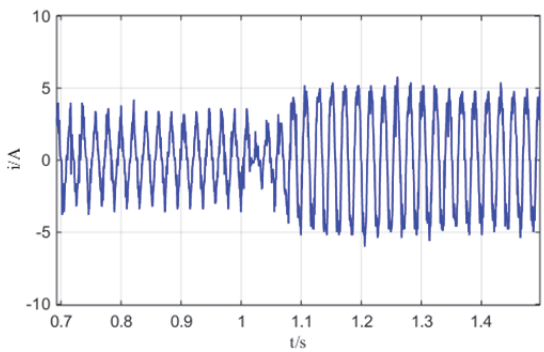

Fig. 15. Experimental waveform of the AC current after load connection.

Simulation and experimental results show that the STATCOM can be used to control the generator terminal voltage rapidly and accurately and to track the reference value on the multi-time scales. The voltage stability and power supply quality of the isolated power system are effectively improved. Fig. 14 and 15 are partially enlarged drawings of the waveform in Fig. 10(b). Fig. 14 shows the dynamical response of the DC voltage u_{dc} after a load connection at 1s. Fig. 15 shows the dynamic response of the A-phase compensation current i_a in the AC time scale and the increase of reactive component with a load connection. In order to ensure the safety of the experiment, an isolation transformer with a transformation ratio of 10 was connected between the STATCOM and the generator. Therefore, the actual DC voltage is 1/10 of its theoretical value.

With reactive power compensation, the terminal voltage remains constant after the load connection, and the voltage and current waveforms of the SEIG remain sinusoidal. Fig. 16 shows that the THD of the terminal voltage and current are both lower than 5% with a load and a STATCOM. Therefore, the proposed modeling and analysis method can ensure stable operation of a device and does not become a harmonic source due to the instability of the control. In addition, the STATCOM's own characteristics, such as the connection inductance, filters out the possible higher harmonics in the current. The frequency was 47Hz due to the limitations of the experimental conditions.

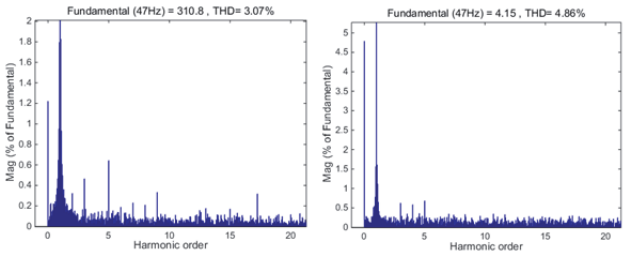

(a) (b)

Fig. 16. Fourier decomposition of experimental waveforms. (a) Fourier decomposition of the terminal voltage. (b) Fourier decomposition of the AC current.

V. CONCLUSIONS

A novel modeling and analysis method for SEIG-STATCOM systems based on the magnitude-phase dynamic method has been proposed in this paper. The application of this method shows the physical mechanism of the device operation. It is convenient to grasp the dynamic characteristics of a STATCOM in different time scales and to estimate the influence of the characteristics of a system on stability in order to regulate the dynamic characteristics. It has been shown that with the magnitude/phase motion equations of the equivalent spring/rotor in the voltage time scale and the current time scale, load changes can be detected rapidly. In addition, the active/reactive component is controlled to track the reference value of voltage or current, resulting in fast terminal voltage regulation. The harmonics generated by the system can be kept within acceptable limits.

ACKNOWLEDGMENT

This financial support provided by National Natural Science Foundation of China (Grant No. 51677092 and 51377086) is acknowledged.

REFERENCES

[1] B. R. Pereira, G. R. M. D. Costa, J. Contreras, and J. R. S. Mantovani, "Optimal distributed generation and reactive power allocation in electrical distribution systems," *IEEE Trans. Sustain. Energy*, Vol. 7, No. 3, pp. 975-984, Jul. 2016.

[2] H. Han, X. C. Hou, J. Yang, J. F. Wu, M. Su, and J. M. Guerrero, "Review of power sharing control strategies for islanding operation of ac microgrids," *IEEE Trans. Smart Grid*, Vol. 7, No. 1, pp. 200-215, Jan. 2016.

[3] D. Wang, X. Z. Wu, J. Q. Chen, Y. J. Guo, and S. W. Cheng, "A distributed magnetic circuit approach to analysis of multiphase induction machines with nonsinusoidal supply," *IEEE Trans. Energy Convers.*, Vol. 30, No. 2, pp. 522-532, Jun. 2015.

[4] Y. W. Wei, L. Y. Kang, Z. Z Huang, Z. Li, and M. M. Cheng, "A magnetic energy recovery switch based terminal voltage regulator for the three-phase self-excited induction generators in renewable energy systems," *J. Power Electron.*, Vol. 15, No. 5, pp. 1305-1317, Sep. 2015.

[5] P. J. Chauhan, J. K. Chatterjee, H. Bhere, and B. V. Perumal, "Synchronized operation of DSP-based generalized impedance controller with variable-speed isolated SEIG for novel voltage and frequency control," *IEEE Trans. Ind. Appl.*, Vol. 51, No. 2, pp. 1845-1854, Mar. 2015.

[6] K. L. V. Iyer, X. Lu, Y. Usama, V. Ramakrishnan, and N. C. Kar, "A twofold daubechies-wavelet- based module for fault detection and voltage regulation in SEIGs for distributed wind power generation," *IEEE Trans. Ind. Electron.*, Vol. 60, No. 4, pp.1638-1651, Apr. 2013.

[7] L. Wang, S. J. Chen, S. R. Jen, and H. W. Li, "Design and implementation of a prototype underwater turbine generator system for renewable micro hydro power energy," *IEEE Trans. Ind. Appl.*, Vol. 49, No. 6, pp. 2753-2760, Nov. 2013.

[8] L. Wang and D. J. Lee. "Coordination control of an AC-to-DC converter and a switched excitation capacitor bank for an autonomous self-excited induction generator in renewable-energy systems," *IEEE Trans. Ind. Appl.*, Vol. 50, No. 4, pp. 2828-2836, Jul. 2014.

[9] M. E. Moursi, K. Goweily, and E. A. Badran, "Enhanced fault ride through performance of self-excited induction generator-based wind park during unbalanced grid operation," *IET Power Electron.*, Vol. 6, No. 8, pp. 1683-1695, Sep. 2013.

[10] M. H. Haque, "Selection of capacitors to regulate voltage of a short-shunt induction generator," *IET Gener., Transm. Distrib.*, Vol. 3, No. 3, pp. 257-265, 2009.

[11] T. Ahmed, O. Noro, E. Hiraki, and M. Nakaoka, "Terminal voltage regulation characteristics by static var compensator for a three-phase self-excited induction generator," *IEEE Trans. Ind. Appl.*, Vol. 40, No. 4, pp. 978-988, Jul. 2004.

[12] S. Rajendran, U. Govindarajan, A. B. Reuben, and A. Srinivasan, "Shunt reactive VAR compensator for grid-connected induction generator in wind energy conversion systems," *IET Power Electron.*, Vol. 6, No. 9, pp. 1872-1883, 2013.

[13] P. S. Sensarma, K. R. Padiyar, and V. Ramanarayanan, "Analysis and performance evaluation of a distribution STATCOM for compensating voltage fluctuations," *IEEE Trans. Power Del.*, Vol. 16, No. 2, pp. 259-264, Apr. 2001.

[14] Y Xu, L. M. Tolbert, J. D. Kueck, and D. T. Rizy, "Voltage and current unbalance compensation using a static var compensator," *IET Power Electron.*, Vol. 3, No. 6, pp. 977-988, Nov. 2010.

[15] N. Mithulananthan, C. Canizares, J. Reeve, and G. J. Rogers, "Comparison of PSS, SVC, and STATCOM controllers for damping power system oscillations," *IEEE Trans. Power Syst.*, Vol. 18, No. 2, pp. 786-792, May 2003.

[16] B. Singh, S. S. Murthy, and S. Gupta, "STATCOM-based voltage regulator for self-excited induction generator feeding nonlinear loads," *IEEE Trans. Ind. Electron.*, Vol. 53, No. 5, pp.1437-1452, Oct. 2006.

[17] B. Singh, S. S. Murthy, and S. Gupta, "Modelling of STATCOM based voltage regulator for self-excited induction generator with dynamic loads," *International Conference on Power Electronics, Drives and Energy Systems* (*PEDES)*, pp. 1-6, 2006.

[18] J. Dalei, K. B. Mohanty, S. Singh, and G. S. Garain, "Fuzzy PI controller for improved voltage regulation in STATCOM based SEIG," *12th IEEE International*

Conference Electronics, Energy, Environment, Communication, Computer, Control (E3-C3), pp. 1-5, 2015.

[19] B. Singh, S. S. Murthy, R. S. Reddy, and P. Arora, "Implementation of modified current synchronous detection method for voltage control of self-excited induction generator," *IET Power Electron.*, Vol. 8, No. 7, pp. 1146-1155, Jul. 2015.

[20] X. M. Yuan, S. J. Cheng, and J. B. Hu, "Multi-time scale voltage and power angle dynamics in power electronics dominated large power systems," *Proc. Chinese Society of Electrical Engineering*, Vol. 36, No. 19, pp. 5145-5154, Oct. 2016.

[21] Y. B. Yan, M. Miao, S. Li, X. M. Yuan, and J. B. Hu, "Current-balancing driven internal voltage motion model of voltage source converter in stationary frame: A physical modeling method in current-control timescale," *Proc. Chinese Society of Electrical Engineering*, Vol. 37, No. 14, pp. 3963-3972, Jul. 2017.

[22] X. Z. Wu, K. S. Hao, and Y. Lan, "Analysis of voltage build-up for self-excited induction generator based on eigenvalues," *Proc. Chinese Society of Electrical Engineering*, Vol. 28, No. 8, pp. 111-116, Mar. 2008.

[23] D. K. Palwalia, "STATCOM-based voltage and frequency regulator for stand-alone asynchronous generator," *International Journal of Power Electronics*, Vol. 6, No. 2, pp. 131-146, Apr. 2014.

[24] H. Yuan, X. M. Yuan, and J. B. Hu, "Modeling and large-signal stability of DFIG wind turbine in dc-voltage control time scale." *IEEE Power and Energy Society General Meeting (PESGM)*, pp. 1-5, 2016.

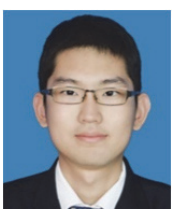

Haifeng Wang was born in Shandong Province, China, in 1992. He received his B.S. degree in Electrical Engineering from the Harbin University of Science and Technology, Rongcheng, China, in 2015. He is presently working towards his M.S. degree in Electrical Engineering at Qingdao University, Qingdao, China. His current research interests include the analysis and control of self-excited induction generator systems.

Xinzhen Wu was born in Jiangsu Province, China, in 1964. He received his B.S. and Ph.D. degrees in Electrical Engineering from Tsinghua University, Beijing, China, in 1986 and 2006, respectively; and his M.S. degree in Electrical Engineering from Southeast University, Nanjing, China, in 1989. He is presently working as a Professor in the Department of Electrical Engineering, Qingdao University, Qingdao, China. His current research interests include the design, analysis and control of electric machines and their systems.

Rui You was born in Qingdao, China, in 1984. He received his B.S. degree in Electrical Engineering from Qingdao University, Qingdao, China, in 2006; his M.S. degree in Electrical Engineering from Shanghai Jiao Tong University, Shanghai, China, in 2009; and his Ph.D. degree in Electrical Engineering from Tsinghua University, Beijing, China, in 2015. He joined Qingdao University in 2015, where he is presently working as an Associate Professor in the Department of Electrical Engineering. His current research interests include wind turbine control and wind power integration.

Jia Li was born in Henan Province, China, in 1980. She received her M.S. degree in Electrical Engineering from Guangxi University, Nanning, China, in 2005. She joined Qingdao University in 2005 as a Teaching Assistant in the Department of Electric Engineering, where she has been a Lecturer since 2007. Her current research interests include self-excited induction generator systems and power system stabilization analysis.